CD49d marks Th1 and Tfh-like antigen-specific CD4$^+$ T cells during *Plasmodium chabaudi* infection

Jiun-Yu Jian[†,‡], Shin-Ichi Inoue[†,‡], Ganchimeg Bayarsaikhan[†], Mana Miyakoda[†,#], Daisuke Kimura[†,#], Kazumi Kimura[†], Eriko Nozaki[§], Takuya Sakurai[¶], Daniel Fernandez-Ruiz[‖], William R. Heath[‖], Katsuyuki Yui[†,‡,††,‡ ‡,¶¶]

[† ‡] Division of Immunology, Department of Molecular Microbiology and Immunology, Graduate School of Biomedical Sciences, Nagasaki University, 1-12-4, Sakamoto, Nagasaki, 852-8523 Japan

[‡] Program for Nurturing Global Leaders in Tropical and Emerging Infectious Diseases, Graduate School of Biomedical Sciences, Nagasaki University, 1-12-4, Sakamoto, Nagasaki 852-8523, Japan

[§]Core Laboratory for Proteomics and Genomics, School of Medicine, Kyorin University, 6-20-2 Shinkawa, Mitaka, Tokyo 181-8611 Japan

[¶]Department of Molecular Predictive Medicine and Sport Science, School of Medicine, Kyorin University, 6-20-2 Shinkawa, Mitaka, Tokyo 181-8611 Japan

[‖]Department of Microbiology and Immunology, The Peter Doherty Institute, The University of Melbourne, Victoria, Australia

[††]School of Tropical Medicine and Global Health, Nagasaki University, 1-12-4, Sakamoto, Nagasaki, 852-8523 Japan

‡ ‡ Institute of Tropical Medicine, Nagasaki University, Nagasaki University, 1-12-4, Sakamoto, Nagasaki, 852-8523 Japan

¶¶Corresponding Author: Katsuyuki Yui, Division of Immunology, Department of Molecular Microbiology and Immunology, Graduate School of Biomedical Sciences, Nagasaki University, 1-12-4, Sakamoto, Nagasaki, 852-8523 Japan. Phone: +81-95-819-7070, FAX: +81-95-819-7073, E-mail: katsu@nagasaki-u.ac.jp

#Present addresses:Daisuke Kimura: Department of Health, Sports, and Nutrition, Faculty of Health and Welfare, Kobe Women's University, 4-7-2 Minatojima-nakamachi, Chuo-ku, Kobe, 650-0046, Japan; Mana Miyakoda: Research and Education Center for Drug Fostering and Evolution, School of Pharmaceutical Sciences, Nagasaki University, 1-14 Bunkyomachi, Nagasaki 852-8521, Japan

Abstract

Upon activation, specific $CD4^+$ T cells upregulate the expression of CD11a and CD49d, surrogate markers of pathogen-specific $CD4^+$ T cells. However, using TCR transgenic mice specific for a *Plasmodium* antigen, termed PbT-II, we found that activated $CD4^+$ T cells develop not only to $CD11a^{hi}CD49d^{hi}$ cells, but also to $CD11a^{hi}CD49d^{lo}$ cells during acute *Plasmodium* infection. $CD49d^{hi}$ PbT-II cells, localized in the red pulp of spleens, expressed transcription factor T-bet, and produced IFN-γ, indicating that they were Th1-type cells. In contrast, $CD49d^{lo}$ PbT-II cells resided in the white pulp/marginal zones and were a heterogeneous population, with approximately half of them expressing CXCR5 and a third expressing Bcl-6, a master regulator of Tfh cells. In adoptive transfer experiments, both $CD49d^{hi}$ and $CD49d^{lo}$ PbT-II cells differentiated into $CD49d^{hi}$ Th1-type cells after stimulation with antigen-pulsed dendritic cells, while $CD49d^{hi}$ and $CD49d^{lo}$ phenotypes were generally maintained in mice infected with *P. chabaudi*. These results suggest that CD49d is expressed on Th1-type *Plasmodium*-specific $CD4^+$ T cells, which are localized in red pulp of the spleen, and can be used as a marker of antigen-specific Th1 $CD4^+$ T cells, rather than that of all pathogen-specific $CD4^+$ T cells.

Key words: malaria, integrin

Introduction

Malaria is a serious health threat with an estimated 229 million cases and 409,000 deaths worldwide in 2019, despite global efforts to control the infection (1). Sporozoites, the infectious form of *Plasmodium* parasites, enter the blood stream via infectious bites by mosquitoes and reach hepatocytes where the parasites expand more than a thousand-fold and develop into merozoites, which repeatedly infect RBCs (2). Symptoms of malaria, such as fever, anemia, and splenomegaly, occur during the blood-stage of malaria when *Plasmodium* parasites repeat cycles of RBC infection and expansion (3, 4). During this stage, specific B cells and $CD4^+$ T cells play critical roles in controlling the infection (5-7). $CD4^+$ T cells are activated by MHC class II-bound peptides derived from *Plasmodium* parasites. The cells proliferate and develop into diverse functional helper T cell subsets including type 1 helper T (Th1) and follicular helper T (Tfh) cells (6, 7). Th1 cells express the key transcription factor T-bet and produce IFN-γ and M-CSF, critical cytokines for controlling *Plasmodium* infection (8). IFN-γ activates macrophages and promotes class switch recombination of B cells during blood-stage *Plasmodium* infection (6,7). M-CSF promotes the function and antigen presenting capacity of myeloid cells (9). Tfh cells are characterized by expression of the key transcription factor Bcl-6, chemokine receptor CXCR5, and high levels of ICOS and PD-1; these cells are essential for the formation of germinal centers, microanatomical sites of B cell maturation and antibody affinity maturation, and promote the maturation of *Plasmodium*-specific germinal center B cells, long-lived plasma cells, and memory B cells (6, 7, 10). However, immunological properties of *Plasmodium* antigen-specific $CD4^+$ T cells during early stage of the infection with *Plasmodium* parasites have not been completely understood.

TCR transgenic mouse expressing TCR specific for *Plasmodium* antigen is a powerful tool to investigate the role of *Plasmodium*-specific $CD4^+$ T cells during blood-stage infection. Stephens et al. generated TCR transgenic mice, B5, expressing TCR specific for *P. chabaudi* MSP-1 antigen in the context of $I\text{-}E^d$ (11). These $CD4^+$ T cells were transferred to BALB/c mice prior to infection with *P. chabaudi*, and these studies illustrated critical roles of *Plasmodium*-specific $CD4^+$ T cells in protective immunity during the transition from acute to chronic phase and during chronic infection (11, 12). Other studies used OVA-specific TCR transgenic mice, OT-II, in combination with transgenic *Plasmodium* parasite expressing recombinant OVA in the cytoplasm (13, 14). These transgenic parasites, however, induce modest specific T cell responses *in vivo* (14, 15). More recently, a TCR transgenic line, termed PbT-II, was created using αβTCR derived from a $CD4^+$ T cell hybridoma generated in response to blood-stage *P. berghei* ANKA infection (16). PbT-II cells recognize *Plasmodium* heat shock protein 90 epitope that is conserved among *P. berghei*, *P. chabaudi*, *P. yoelii*, and *P. falciparum* in the context of $I\text{-}A^b$ (Enders et al, submitted for publication). Transfer of PbT-II cells into CD40L deficient mice promoted antibody response to the subsequent *P. chabaudi* infection, thus controlling otherwise lethal infection. This TCR transgenic mouse model was used for a single-cell transcriptome analysis during blood-stage infection with *P. chabaudi* to characterize the development of effector $CD4^+$ T cells at a single-cell level (17). The study showed that activated $CD4^+$ T cells bifurcate and develop simultaneously into Th1 and Tfh cell types during *Plasmodium* infection and suggested that this bifurcation is affected by the interaction of activated $CD4^+$ T cells with B cells as well as myeloid cells.

Another approach to identify specific $CD4^+$ T cells during infection is the use of cell surface markers whose expression is altered upon activation of T cells in response to pathogen-derived antigens. Antigen-specific $CD4^+$ T cells upregulate CD11a and CD49d expression

after infection by lymphocytic choriomeningitis virus (LCMV), *Listeria monocytogenes*, and *Plasmodium* parasites. Therefore, detecting their expression is useful in identifying antigen-specific $CD4^+$ T cells (18-21). All $CD4^+$ T cells producing IFN-γ in response to pathogens are of the $CD11a^{hi}CD49d^{hi}$ phenotype and have been shown to stably express these molecules in memory phase. Furthermore, the proportion of $CD11a^{hi}CD49d^{hi}$ $CD4^+$ T cells was observed to increase during a human vaccine trial, and all $CD4^+$ T cells producing effector cytokines, including IFN-γ, were present within this population, suggesting that these surrogate markers of antigen-specific $CD4^+$ T cells can also be applied to humans (22).

In the current study, we investigated cell surface markers of *Plasmodium*-specific $CD4^+$ T cells during early activation with blood-stage *P. chabaudi* infection using a PbT-II TCR transgenic mouse model (16). Although CD11a was upregulated in all PbT-II cells in the infected mice, CD49d was unregulated only in a subset of PbT-II cells. $CD11a^{hi}CD49d^{hi}$ and $CD11a^{hi}CD49d^{lo}$ PbT-II cells localized to a distinct tissue compartment in the spleen of *P. chabaudi* infected mice and exhibited differences in the gene expression profiles and function. Characterization of these two subsets of $CD4^+$ T cells suggested that $CD11a^{hi}CD49d^{hi}$ are Th1, while $CD11a^{hi}CD49d^{lo}$PbT-II cells contain multiple cell types, including Tfh cells.

Methods

Mice and parasites

PbT-II transgenic mice expressing the TCR specific for *Plasmodium* antigen associated with I-A^b (16) were bred with B6.SJL (CD45.1) mice and the offspring were intercrossed to obtain CD45.1 PbT-II mice. C57BL/6 mice were purchased from SLC (Shizuoka, Japan). Mice were maintained in the Laboratory Animal Center for Animal Research at the Nagasaki University. Mice were used at 7–10 weeks of age. The animal experiments were approved by the Institutional Animal Care and Use Committee of Nagasaki University and were conducted according to the guidelines for Animal Experimentation of Nagasaki University.

Plasmodium chabaudi chabaudi AS was provided by Dr. R. Culleton (Ehime University, Ehime, Japan). Experimental mice were infected intraperitoneally (i.p.) with parasitized RBCs (5×10^4) from mice that were previously passed from a frozen stock. Parasitemia was determined by either microscopic standard thin blood smears with a Diff-Quick staining kit (Sysmex, Kobe, Japan) or using flow cytometry in which blood obtained from tail veins was stained with Hoechst 33342 (8 µM; Sigma-Aldrich, St. Louis, MO, USA), dihydroethidium (diHEt, 10 µg/mL) as described in a previous study (23). Cells were analyzed on a BD LSRFortessa X-20 cell analyzer (BD Bioscience, San Diego, CA, USA) and FlowJo software version 10.4 (Tree Star Technologies, Ashland, OR, USA).

Adoptive transfer of PbT-II cells

PbT-II $CD4^+$ T cells (>95%) were prepared from a pool of spleens and brachial and inguinal lymph nodes using anti-CD4 IMag magnetic beads (BD Biosciences) as described in a previous study (24). C57BL/6 mice were adoptively transferred with PbT-II cells (1×10^6) via i.v. injection in the tail vein and were infected with *P. chabaudi* i.p. on the same day. In some of the experiments, PbT-II cells were labeled with CFSE (15 µM; Invitrogen, Carlsbad, CA, USA) for 10 min in PBS containing 1% bovine serum albumin (BSA) as described in a previous study (24). After washing 3 times, CFSE-labeled cells were resuspended in PBS and transferred via i.v. injection into C57BL/6 mice. Proliferation of PbT-II cells was monitored by diminution of CFSE using an LSRFortessa X-20 cell analyzer (BD Biosciences) and FlowJo software.

Flow cytometry

Spleen cells were treated with Gey's solution to lyse RBCs. Peripheral blood (100 µL) was collected from the right submandibular vein of the mice, mixed with heparin (1 unit), and treated with Gey's solution. Cells were stained for cell surface molecules using monoclonal antibodies (mAb) for 30 min at 4 °C. Antibodies used for flow cytometry analysis were purchased from Biolegend (San Diego, CA, USA), Tonbo Biosciences (San Diego, CA, USA.), eBioscience (San Diego, CA, USA), and BD Biosciences. Next, 7-aminoactinomycin D (7-AAD) was added to exclude dead cells and the samples were analyzed using the LSRFortessa X-20 cell analyzer and FlowJo software. Forward scatter FSC-H vs. FSC-W and side scatter SSC-H vs. SSC-W were used to exclude doublets. Quadrants were determined based on the staining of isotype control antibodies. For intracellular staining of transcription factors, splenocytes were treated with anti-Fcγ receptor mAb (2.4G2), stained for surface

markers, fixed, permeabilized using a Foxp3/Transcription Factor Staining Buffer set (eBioscience), and stained with specific mAbs following the manufacturer's instructions. For intracellular cytokine staining, splenocytes (3×10^6) were resuspended in RPMI-1640 supplemented with glutamine (2mM), penicillin/streptomycin, non-essential amino acids (0.1 mM), sodium pyruvate (1 mM), 2-mercaptoethanol (5×10^{-5} M), and 10% heat-inactivated fetal calf serum (R10 medium) and cultured in 24 well plates for 4 h in the presence of BD GolgiStop™ following the manufacturer's instructions with slight modifications (25). Cells were stimulated with either phorbol 12-myristate 13-acetate (PMA, 20 ng/mL) and ionomycin (1 µg/mL) or PbT-II peptide (DNQKDIYYITGESINAVS) (1 µM) (Enders et al, submitted for publication). The peptide was custom synthesized by SIGMA Genosys (Sigma-Aldrich Japan, Tokyo, Japan). Cells were then incubated with anti-Fcγ receptor mAb, stained for CD4, CD3, CD45.1, CD11a, or CD49d, washed, fixed and permeabilized using a BD Cytofix/Cytoperm™ PlusFixation/Permeabilization Kit (BD Biosciences), and stained for IFN-γ, IL-2, TNF-α , and IL-10. To distinguish cells in the red pulp (RP) and white pulp (WP) of the spleen, mice received PE-anti-CD45.1 mAb (3 µg, A20) via i.v. injection and were euthanized 3 min later. The spleens were harvested and the RBCs were lysed using Gey's solution. Splenocytes were stained for CD45.2, CD4, CD11a, CD49d, TCR Vα 2, or their isotype controls. Stained cells were analyzed using the LSRFortessa X-20 cell analyzer and FlowJo software.

Cell sorting

C57BL/6 mice were adoptively transferred with PbT-II cells and then infected with *P. chabaudi*. Seven days later, CD45.1$^+$PbT-II cells were enriched from spleens using MACS beads (Miltenyi Biotec, Gladbach, Germany) following the manufacturer's instructions with slight modifications (25). Briefly, splenocytes were stained with APC-anti-CD45.1 mAb, washed, incubated with anti-APC MACS beads for 30 min at 4 °C, washed, and enriched

using an autoMACS Pro Separator (Miltenyi Biotec). Enriched cells were further stained for CD3, CD4, CD11a, or CD49d and sorted using a FACSAria II cell sorter (BD Biosciences) to collect $CD11a^{hi}CD49d^{hi}$ and $CD11a^{hi}CD49d^{lo}$ PbT-II ($CD45.1^{+}CD3^{+}CD4^{+}$) cells.

ELISA

To examine antigen-specific responses, sorted $CD11a^{hi}CD49d^{hi}$ and $CD11a^{hi}CD49d^{lo}$ PbT-II cells (5×10^{3}) were suspended in R10 medium and cultured in 96-well flat-bottom plates with splenocytes (5×10^{5}) from uninfected C57BL/6 mice in the presence or absence of PbT-II peptide. The levels of IFN-γ and IL-2 in the culture supernatant were determined via sandwich ELISA using anti-IFN-γ and biotin-anti-IFN-γ mAbs or anti-IL-2 and biotin-anti-IL-2 mAbs, respectively. The levels of IL-10 and TNF-α were determined using Ready-SET-Go! ELISA kits (eBioscience) following by the instruction manual.

Immunohistochemistry and confocal microscopy

Immunohistochemical analysis was performed as previously described with slight modification (25). Briefly, spleens were snap frozen and then embedded in Tissue-Tek OCT compound (Sakura Finetek, Tokyo, Japan) in a dry ice-methanol bath. Five μm thick sections of tissue specimens were cut using a cryomicrotome (Leica, Germany) and fixed with acetone for 15 min at room temperature. Samples were blocked using Blocking One Histo (Nacalai, Kyoto, Japan) for 1 h in a humidity chamber at room temperature. Sections were then stained with PE-anti-CD45.1, FITC-anti-CD169, and biotin-anti-CD49d mAbs overnight at 4 °C. Sections were washed and stained with Cy5-streptavidin (BioLegend). Samples were mounted in DAKO fluorescent mounting medium (Agilent Technologies, Santa Clara, CA, USA) and images were acquired using an LSM 800 confocal microscope system (Carl Zeiss, Jena, Germany) and merged using the ImageJ software (National Institutes of Health,

Bethesda, MD, USA). The number of PbT-II cells in RP, WP, or marginal zone (MZ) were counted in a 0.5 mm^2 area of a microscopic field. Statistical analysis was performed on 15 different areas from each spleen and three different mice were examined.

Microarray analysis

Total RNA was prepared from purified T cells using an RNeasy Mini Kit (Qiagen, Hilden, Germany). The quality and concentration of the RNA were evaluated using an Agilent Tapesation 2200 system (Agilent Technologies). RNA samples with RNA integrity numbers higher than 7 were used for subsequent assays. Synthesis of complementary DNA (cDNA) from the total RNA (2 ng), its amplification, fragmentation, and labeling were performed using a GeneChip 3' IVT Pico Kit (Applied Biosystems) according to the manufacturer's instructions. Gene-expression profiles of the amplified cDNA (6.6 μg/array) were determined using the Clariom S Array, mouse (Applied Biosystems). Subsequent analysis was performed using the Transcriptome Analysis Console software (Invitrogen) to evaluate gene expression levels. Differentially expressed genes were listed for those with at least 2-fold changes and *p* values < 0.05 compared between the $CD11a^{hi}CD49d^{hi}$ and $CD11a^{hi}CD49d^{lo}$ cells. Software for Gene Set Enrichment Analysis (GSEA) (26) was downloaded from the home page of the Broad Institute (Massachusetts Institute of Technology, Cambridge, MA, USA) and obtained data were compared with those from the Molecular Signatures Database (MSigDB) (26). Data were processed in R using either its basic function or the package ggplot2 (27) and pheatmap (28) to visualize the results. The microarray datasets generated during this study are available at GSE/microarray data (GSE153600).

Bone marrow-derived dendritic cells (BM-DCs)

Granulocyte-macrophage colony-stimulating factor (GM-CSF)-supplemented BM culture was performed as described in a previous study (29). Briefly, BM cells from C57BL/6 mice were cultured (2×10^5 cells/ml) in 10 ml of R10 medium supplemented with GM-CSF (200 U; BioLegend). On day three, 10 mL of R10 medium and GM-CSF (200 U) were added. On day 6, 10 ml of R10 medium and GM-CSF was replaced and lipopolysaccharide (LPS) derived from *Escherichia coli* 0127:B8 (Sigma) was added at a final concentration of 20 ng/ml. After 24 h, the cells were washed, centrifuged, counted, and pulsed with PbT-II peptide (1 μM) for 3 h. Cells were washed, resuspended in PBS, and inoculated via i.v. injection (2.5×10^5cells/mouse) one day after transfer of PbT-II cells.

Statistical analysis

Data were analyzed using the GraphPad Prism software (Prism 8, La Jolla, CA, USA). For comparisons between two groups, two-tailed unpaired Student's *t* tests were used. When three or more groups were compared, an overall difference between the groups was determined using ANOVA or two-way ANOVA. When one-way or two-way ANOVA was significant, differences between individual groups were estimated using post-hoc Tukey's test.

Results

Proliferation of CD11a^{hi}CD49d^{hi} and CD11a^{hi}CD49d^{lo} PbT-II cells after *P.chabaudi* infection

To determine the response of *Plasmodium* antigen-specific CD4$^+$ T cells during infection with *P. chabaudi*, C57BL/6 mice received a transfer of PbT-II cells and were then infected with *P. chabaudi*. Seven to 30 d after infection, the proportions of PbT-II cells among CD4$^+$ T cells in spleens and peripheral blood lymphocytes (PBLs) were determined and their CD11a and CD49d expression levels were examined (Figure 1, Figure S1A). The proportion of PbT-II cells increased dramatically in both the spleen and PBLs 7 d after infection with *P. chabaudi* and gradually decreased with concurrent reduction in parasitemia levels (Figure 1B, 1C). In the spleen, on day 7, 28.0 ± 2.8 % of PbT-II cells expressed high levels of both CD11a and CD49d, whereas 52.5 ± 2.5 % of PbT-II cells exhibited the CD11a^{hi}CD49d^{lo} phenotype (Figure 1C). The proportion of CD11a^{hi}CD49d^{hi} PbT-II cells gradually declined in parallel with the reduction in total PbT-II proportions, while that of CD11a^{hi}CD49d^{lo} was maintained in the spleen after 7 d of infection. Interestingly, a majority of the PbT-II cells (70.1 ± 3.7 %) among PBLs were of the CD11a^{hi}CD49d^{hi} phenotype 7 d after infection, but the number rapidly decreased thereafter (Figure 1C). In host compartments, 19.1 ± 2.7 % and 27.2 ± 3.9 % of CD4$^+$ T cells were of the CD11a^{hi}CD49d^{hi} phenotype in spleens and PBLs, respectively, on day 7 of infection and their proportions continuously declined in a manner similar to that of PbT-II cells (Figure S1B, S1C). The proportions of CD11a^{hi}CD49d^{lo} CD4$^+$ T cells were relatively stable in the spleen during 7–30 d of infection while those in the PBLs were at low levels. CD11a^{hi}CD49d^{hi} and CD11a^{hi}CD49d^{lo} PbT-II cells were also detected in mice infected with *P. yoelii* (Figure S2A).

We first considered whether CD11a^{hi}CD49d^{lo} cells were an intermediate stage of activation and differentiation in the pathway to the development of CD11a^{hi}CD49d^{hi} CD4^{+} T cells. Alternatively, we also postulated that these two populations might be independent lineages of CD4^{+} T cells. To this end, CFSE-labeled PbT-II cells were transferred into C57BL/6 mice and proliferation of CD11a^{hi}CD49d^{hi} and CD11a^{hi}CD49d^{lo} PbT-II cells was monitored after infecting the mice with *P. chabaudi* (Figure 2A). The proportion of PbT-II cells increased concomitantly with the increase in parasitemia and both CD11a^{hi}CD49d^{hi} and CD11a^{hi}CD49d^{lo} PbT-II cells exhibited similar numbers of divisions, whereas CD11a^{lo}CD49d^{lo} cells did not divide (Figure 2B). This suggested that CD11a^{hi}CD49d^{lo} cells are unlikely to be intermediate pathway to the development of CD11a^{hi}CD49d^{hi} CD4^{+} T cells.

CD11a^{hi}CD49d^{hi} and CD11a^{hi}CD49d^{lo} PbT-II cells localize in different splenic compartments

Phenotypical analysis of PbT-II cells indicated that CD11a^{hi}CD49d^{lo} cells increased in the spleen, but not in PBLs after *P. chabaudi* infection (Figure 1). CD49d is an α4 subunit of the integrin chains and combines with β1 (CD29) and β7 to form very late antigen 4 (VLA-4) and LPAM-1, respectively, which have critical roles in the control of cell migration (30). Therefore, we hypothesized that CD11a^{hi}CD49d^{hi} and CD11a^{hi}CD49d^{lo} populations would localize in different tissue compartments. To determine the distribution of PbT-II cells in the spleen, we stained the cells *in vivo* via i.v. injection of PE-labeled anti-CD45.1 mAb 3 min prior to euthanasia (Figure 3A). The injected mAb could reach the RP/MZ, but not the WP (25, 31). The proportion of CD11a^{hi}CD49d^{hi} PbT-II cells that were stained with the anti-CD45.1 mAb was 75.5 ± 2.8%, whereas that of CD11a^{hi}CD49d^{lo} PbT-II cells was 17.1 ± 1.3 %, implying that CD11a^{hi}CD49d^{hi} PbT-II cells localized mainly in the RP/MZ while CD11a^{hi}CD49d^{lo} PbT-II cells localized mainly in the WP. To directly determine their

localization, we examined splenic tissue using histochemical analysis (Figure 3B). PbT-II cells were detected in both RP and WP. However, the majority of the PbT-II cells in the WP were CD49d^{lo} whereas the majority of those in the RP were CD49d^{hi}, supporting the idea that CD11a^{hi}CD49d^{hi} PbT-II cells are mainly localized to the splenic RP, while CD11a^{hi}CD49d^{lo} PbT-II cells reside in the WP.

Transcriptional profiles of CD49d^{hi} and CD49d^{lo} PbT-II cells in *P. chabaudi*-infected mice

To examine the relationships between CD11a^{hi}CD49d^{hi} and CD11a^{hi}CD49d^{lo} PbT-II cells in *P. chabaudi*-infected mice, we performed gene expression profiling of these populations, as well as of naïve CD11a^{lo}CD49d^{lo} PbT-II cells, using microarray analysis. Principal component (PC) analysis revealed that CD11a^{hi}CD49d^{hi} and CD11a^{hi}CD49d^{lo} PbT-II cells were set apart from naïve PbT-II cells along PC1 and separated from each other primarily along PC2 (Figure 4A). Upon comparing CD11a^{hi}CD49d^{hi} PbT-II cells to CD11a^{hi}CD49d^{lo} PbT-II cells, we identified 681 upregulated genes and 1,081 downregulated genes ($p < 0.05$, Log2 fold change ≥ 2; Figure 4B, 3C). *Tbx21*, *Ifnγ*, *Cxcr6*, *Ly6C1*, *Ly6C2*, *Ifng1*, *Ccl5*, *Gzmb*, and *Lgals3* were among the upregulated genes. *Lgals3*, which encodes galectin-3, was consistent with single-cell analysis of Th1-type PbT-II cells (17). In contrast, the upregulated genes in CD11a^{hi}CD49d^{lo} PbT-II cells included *Il6ra*, *Tcf7*, *Cd200*, *Bcl6*, *Cxcr5*, *Egr2*, *Egr3*, and *Stat6*, which are associated with Tfh cell differentiation. *Tcf7* is expressed in naïve and activated T cells and blocks the differentiation into Th1 by negatively regulating IFN-γ expression and promoting early priming of Tfh cells by directly binding to the promoters of Tfh associated genes (32-34). *Egr2* is induced after T cell activation and promotes Tfh differentiation in conjunction with *Egr3* (35). *Tox*, critical transcription factor for CD8^{+} T cell exhaustion, was also upregulated in CD11a^{hi} PbT-II cells (36, 37). Gene set enrichment

analysis of the upregulated genes in CD11a^{hi}CD49d^{hi} PbT-II cells against those from MSigDB (26) revealed enrichment of the gene set associated with Th1 cells, while upregulated genes in CD11a^{hi}CD49d^{lo} PbT-II cells were enriched with the gene set associated with Tfh cells (Figure 4D). These findings suggested that the expression of CD49d distinguished Th1 and Tfh cells during *Plasmodium* infection.

Phenotype and cytokine production of CD49d^{hi} and CD49d^{lo} PbT-II cells

To confirm Th1 and Tfh properties of CD49d^{hi} and CD49d^{lo} PbT-II cells in *P. chabaudi*-infected mice, we characterized their phenotypes and functions. C57BL/6 mice were injected with PbT-II cells and infected with *P. chabaudi*. PbT-II cells were then harvested 7 d after infection and the expression of surface markers and transcription factors in CD49d^{hi} and CD49d^{lo} PbT-II cells was determined (Figure 5, Figure S3). CD49d^{hi} PbT-II cells expressed higher levels of inhibitory receptors PD-1, LAG3, TIM-3, and CTLA-4, PD-L1, and Ly6C, whereas CD49d^{lo} PbT-II cells expressed higher levels of CXCR5. These makers were also expressed on host CD11a^{hi}CD49d^{hi} and CD11a^{hi}CD49d^{lo} CD4^{+} T cells (Figure 5B). Regarding transcription factors, the majority of CD49d^{hi} PbT-II cells expressed high levels of T-bet and Blimp1, suggesting that they were Th1 cells. The expression of Tfh-type transcription factors in CD49d^{lo} PbT-II cells was more heterogeneous, with 92.6% being Tcf1^{+}, 72.8% being Egr2^{+}, and 36.6% being Bcl6^{+}, suggesting that this population of cells comprised multiple cell types including Tfh cells. Host CD11a^{hi}CD49d^{hi} and CD11a^{hi}CD49d^{lo} CD4^{+} T cells also expressed Th1 and Tfh transcription factors, respectively. Analysis of CD4^{+} T cells from mice infected with *P. yoelii* also showed that CD49d^{hi} PbT-II cells are Th1 type and CD49d^{lo} PbT-II contain Tfh-like cells (Figure S2B). Taken together, these results confirmed that CD11a^{hi}CD49d^{hi} CD4^{+} T cells in *Plasmodium*-infected mice were Th1 cells and CD11a^{hi}CD49d^{lo} cells consisted of a heterogeneous population including Tfh lineage.

Next, we examined cytokine production by CD49d^{hi} and CD49d^{lo} PbT-II cells in response to TCR stimulation. The two populations were sorted and stimulated with DCs pulsed with antigenic peptide (Figure 6A). CD49d^{hi} PbT-II cells produced higher levels of IFN-γ and IL-10 and lower levels of IL-2 as compared with CD49d^{lo} PbT-II cells. There was no significant difference in the production of TNF-α. Intracellular cytokine staining showed that the majority of CD49d^{hi} PbT-II cells uniformly produced high levels of IFN-γ in response to PMA and ionomycin, as well as to PbT-II peptide (Figure 6B, Figure S4A). Additionally, ~60% of the cells co-produced TNF-α, ~30% co-produced IL-10, and ~26% co-produced IL-2 in response to PMA and ionomycin. In contrast, CD49d^{lo} PbT-II cells included at least two subpopulations that exhibited distinct patterns of cytokine production. Approximately half of the CD49d^{lo} PbT-II cells expressed IFN-γ, TNF-α, and IL-2, but not IL-10, in response to PMA and ionomycin. The remaining CD49d^{lo} PbT-II cells failed to produce any of these cytokines, except for low levels of TNF-α and IL-2. In the host CD4^{+} T cell compartment, CD11a^{hi}CD49d^{hi} cells exhibited high IFN-γ production while CD11a^{hi}CD49d^{lo} cells consisted of two types, one producing IFN-γ and the other not producing IFN-γ, similar to PbT-II cells (Figure S4). These functional studies confirmed that CD49d^{hi} PbT-II cells were Th1-type cells, including IL-10-producing Tr1 cells, while CD49d^{lo} PbT-II cells consisted of a more heterogeneous population.

Development of CD49d^{lo} PbT-II cells into functional CD49d^{hi} cells

To clarify the relationship between CD49d^{hi} and CD49d^{lo} PbT-II cells, we sorted both populations of cells from *P. chabaudi*-infected mice, transferred them into C57BL/6 mice, and stimulated them *in vivo* with BM-DCs pulsed with PbT-II peptide (Figure 7). The proportions of CD49d^{hi}-derived and CD49d^{lo}-derived PbT-II cells of the total CD4^{+} T cells

were 2.4 ± 0.9% and 2.1 ± 0.5%, respectively, on day 5 after stimulation, suggesting that both populations expanded similarly *in vivo* in response to the antigen (Figure 7C, 7D). As early as 2 days after stimulation, 68.4 ± 4.1% of CD49d^{lo}-derived PbT-II cells displayed the CD11a^{hi}CD49d^{hi} phenotype, similar to 75.3 ± 2.2% of CD49d^{hi}-derived PbT-II cells (Figure 7B, 7D). The upregulation of CD49d did not occur in CD49d^{lo}-derived PbT-II cells without antigen stimulation (Figure S4C). Both CD49d^{hi}-and CD49d^{lo}-derived PbT-II cells barely expressed PD-1 and LAG-3. Interestingly, the proportion of CD49d^{lo}-derived PbT-II cells expressing Ly6C was not as high as that of CD49d^{hi}-derived PbT-II cells. However, both CD49d^{hi}-derived and CD49d^{lo}-derived PbT-II cells produced IFN-γ as well as IL-2 after stimulation with PMA and ionomycin or with PbT-II peptide (Figure 7). These data suggest that CD49d^{lo} PbT-II cells in *Plasmodium*-infected mice have the potential to become CD11a^{hi}CD49d^{hi} IFN-γ-producing Th1 type CD4^{+} T cells when they are stimulated by activated conventional DCs.

We further evaluated the fate of CD49d^{hi} and CD49d^{lo} PbT-II cells in the environment of *P. chabaudi* infection. CD49d^{hi} and CD49d^{lo} PbT-II cells were prepared from *P. chabaudi*-infected mice, transferred into 5 d-infected C57BL/6 mice, and the splenic CD4^{+} T cells were analyzed 2 d later (Figure 8). The proportion of CD49d^{lo}-derived PbT-II cells (0.4 ± 0.3%) was higher than that of CD49d^{hi}-derived PbT-II cells (0.1 ± 0.04%), suggesting that CD49d^{lo}-derived PbT-II cells had a higher potential to multiply than CD49d^{hi} PbT-II cells under the infection environment. Phenotypically, 44.5 ± 3.2% of the CD49d^{hi}-derived PbT-II cells remained CD11a^{hi}CD49^{hi} with the majority expressing Ly6C (51.0 ± 2.3%) and LAG3 (53.0 ± 0.8%), while some became CD11a^{hi}CD49^{lo} (30.6 ± 4.0%) and CXCR5^{+} (41.8 ± 4.0%), suggesting that CD49d^{hi} CD4^{+} T cells contain cells that could differentiate to Tfh-like cells during blood-stage *Plasmodium* infection. In contrast, 51.3 ± 7.1% of the CD49d^{lo} PbT-II

cells remained CD11a^{hi}CD49d^{lo} with the majority being CXCR5^{+} (72.0 ± 1.1%), while their subpopulation was CD11a^{hi}CD49^{hi} (19.7 ± 4.8%) and Ly6C^{+} (27.4 ± 2.6 %), suggesting that the CD11a^{hi}CD49d^{lo} phenotype of *Plasmodium*-specific CD4^{+} T cells was relatively stable during the *Plasmodium*-infection, when compared with those stimulated with antigen-pulsed BM-DCs.

Discussion

CD11a and CD49d integrin molecules have been used as surrogate markers of antigen-specific CD4^{+} T cells (18, 19, 21). In the current study, we used PbT-II, which were *Plasmodium*-antigen-specific TCR transgenic mice, and found that CD49d expression was heterogeneous in *Plasmodium*-specific CD4^{+} T cells, along with distinguishing those with different localization and functions. CD49d^{hi} PbT-II cells localized within the splenic RP and PBLs expressed the transcription factor T-bet, and produced IFN-γ in response to TCR stimulation, indicating that they were Th1 cells. In contrast, CD49d^{lo} PbT-II cells were localized to WP and comprised heterogeneous populations that included Tfh cells. Approximately half of the CD49d^{lo} PbT-II cells expressed CXCR5 and a third expressed Bcl-6, a master regulator of Tfh (10, 38, 39), while the majority expressed transcription factors TCF1 and Egr2, which inhibit differentiation towards Th1 and promote Tfh fate (32, 34, 40). These outcomes suggest that the expression of CD49d is associated with differentiation of CD4^{+} T cells into Th1 cells, rather than their specific activation as described previously (18-21).

Our study showed that the expression of CD49d was associated with the differentiation of PbT-II cells into Th1 type and their localization in the spleen RP during *Plasmodium* infection, while CD49d^{lo} PbT-II cells remained in WP. CD49d is the α4-integrin subunit that generates VLA-4 (CD49d/CD29) in association with CD29 (β1 chain) and binds to vascular

cell adhesion molecule (VCAM)-1, and binds to the mucosal address in cell adhesion molecule (MAdCAM)-1 in conjunction with the β7 molecule (41). The α4-integrins also interact with fibronectin in the tissue. Anti-α4-integrin antibody inhibits trafficking of pathogenic cells through the blood-brain barrier into the central nervous system and is used for the treatment of multiple sclerosis (42, 43). The expression of adhesion molecules and chemokine receptors likely affects the distribution of activated $CD4^+$ T cells in RP vs WP. To determine whether CD49d plays an active role in the localization and development of $CD4^+$ T cells that express it, we performed an *in vivo* blockade of CD49d with an antibody during *Plasmodium* infection. However, we were unable to obtain evidence suggesting the effect of CD49d blockade on the generation of Th1 and other effector T cells (data not shown). Therefore, we speculate that CD49d expression is not a primary determining factor for Th1 differentiation. It remains possible, however, that the CD49d molecule on activated $CD4^+$ T cells is involved in their interaction with antigen-presenting cells or with splenic tissue and promotes the differentiation of $CD4^+$ T cells towards Th1 cells during *Plasmodium* infection. Further study is required to determine the role of CD49d on $CD4^+$ T cells during *Plasmodium* infection.

$CD49d^{lo}$ PbT-II cells were a heterogeneous population of mostly T-$bet^{lo}Tcf1^{hi}$ phenotype and included Tfh-like cells that expressed CXCR5 and Bcl-6. This population became $CD49d^{hi}$ as early as 2 days after being transferred into naïve mice followed by stimulation with antigen-pulsed BM-DCs and developed into functional Th1 cells. Although it is not clear which subpopulation within $CD49d^{lo}$ PbT-II cells developed into Th1 cells, we think that it is not a small population, since this transition occurred in a short period of time after stimulation with antigen pulsed BM-DCs. The plasticity of memory $CD4^+$ subsets in recall responses has been previously reported (44, 45). During *Plasmodium* infection, memory Th1-like cells have the

plasticity to give raise to Tfh-like secondary effectors following adoptive transfer and recall response to homologous challenge infection with recombinant *P. yoelii* expressing a model antigen epitope (44). Alternatively, long-lived Tfh-like memory cells give rise to both Th1 and Tfh effectors in recall responses to challenge infection with homologous parasites in a lymphocytic choriomeningitis infection model (45). We also observed plasticity of CD49d^{hi} as well as CD49d^{lo} PbT-II cells during *Plasmodium* infection. However, CD49d^{lo} PbT-II cells better maintained their properties after transfer into *P. chabaudi*-infected mice when compared with those transferred and stimulated with antigen-pulsed BM-DCs. We were able to track the transferred PbT-II cells in *Plasmodium*-infected mice for only two days as the limited expansion of these cells was surpassed by the expanding innate immune cells in the spleen at this stage, which resulted in the poor recovery of PbT-II cells. With this caveat of a short duration, the results of our transfer experiments suggested that activated specific CD4$^+$ T cells developed into Th1 and Tfh-like effector cells and relatively maintained their properties during acute *Plasmodium* infection. We think that it is likely that the tissue environment of *Plasmodium* infection is suitable for the differentiation and maintenance of these functional CD4$^+$ T cell subsets. Furthermore, our current results are consistent with the fact that CD49d expression is a reliable marker of Th1-type CD4$^+$ T cells for evaluating CD4$^+$ T cell functional subtypes during *Plasmodium* infection.

Our study showed bifurcation of *Plasmodium*-specific CD4$^+$ T cells to Th1 and Tfh-like cells during acute malaria, which is consistent with a previous single-cell transcriptional analysis of *Plasmodium*-specific CD4$^+$ T cells (17). IFN-γ and *Plasmodium*-specific antibodies were shown to be critical for protective immunity against blood-stage *Plasmodium* infection in rodent models and human malaria. However, the protective immune response during blood-stage *Plasmodium* infection is often ineffective leading to chronic infection, and the roles of

specific Th1 and Tfh cells in the protection against *Plasmodium* infection are not clearly understood (6, 7). IFN-γ is produced not only by *Plasmodium*-specific Th1 cells but also by $CD8^+$ T cells, NK cells and γδ cells, and it is not clear which source is critical for the protection *in vivo* (7). Furthermore, Th1 and Tfh cells interact with each other during immune responses and excessive IFN-γ produced by Th1 cells restricts the generation of Tfh cells and is detrimental to the generation of humoral immunity in response to *Plasmodium* infection (46). Finally, in human malaria cases, circulating Tfh-type subsets are detectable in PBLs of Malian children living in an endemic area, and acute malaria infection preferentially activates less-functional Th1-polarized Tfh cells resulting in the lack of correlation between circulating Tfh responses and B-cell and antibody responses (47). These features point to the complex nature of the immune response to *Plasmodium* infection and the requirement for molecular markers that correlate with the protective ability of immune responses against *Plasmodium* infection. It remains to be determined whether CD49d expression is maintained during chronic malaria infection and whether it can be used as a stable marker for functional $CD4^+$ T cell subsets in rodent and human malaria. Further study is required to determine the usefulness of CD49d expression in defining functional subsets of specific $CD4^+$ T cells during the course of *Plasmodium* infection as well as in other immune activation conditions including vaccination, and whether its expression on $CD4^+$ T cells correlates with the protective ability of the immune responses. Finally, the study suggests that defining the mechanisms underlying the role of integrin molecules in determining T cell fate is important in comprehending the to resolve the regulation of T cell differentiation.

Funding

This work was supported by Grants-in-Aid for Scientific Research from the Japan Society for the Promotion of Science [grant number 18K07094 to S.I. and 18K19456, 19H03460, 19KK0207 to K.Y.], the Ohyama Health Foundation Inc. to S.I., the Takeda Science Foundation to S.I., and National Health and Medical Research Council of Australia [grant number 1113293, 1139486, 1154457] to WRH and DF-R.

Acknowledgements

We thank Dr. Yi-Ting Lai (Academia Sinica, Taipei, Taiwan) for helping with confocal software adjustments and for instructions regarding image analysis and Ms. N. Kawamoto for technical help. We would like to thank Editage for English language editing.

Conflicts of interest statement: the authors declared no conflicts of interest.

References

1. WHO. 2020. World malaria reprot 2020. *https://www.who.int/publications/i/item/9789240015791*.
2. Cowman, A. F., J. Healer, D. Marapana, and K. Marsh. 2016. Malaria: Biology and Disease. *Cell* 167: 610-624.
3. Haldar, K., S. C. Murphy, D. A. Milner, and T. E. Taylor. 2007. Malaria: mechanisms of erythrocytic infection and pathological correlates of severe disease. *Annu Rev Pathol* 2: 217-249.
4. Yui, K., and S. I. Inoue. 2020. Host-pathogen interaction in the tissue environment during *Plasmodium* blood-stage infection. *Parasite Immunol*: e12763.
5. Hafalla, J. C., O. Silvie, and K. Matuschewski. 2011. Cell biology and immunology of malaria. *Immunol Rev* 240: 297-316.
6. Kurup, S. P., N. S. Butler, and J. T. Harty. 2019. T cell-mediated immunity to malaria. *Nat Rev Immunol* 19: 457-471.
7. Kumar, R., J. R. Loughland, S. S. Ng, M. J. Boyle, and C. R. Engwerda. 2020. The regulation of $CD4^+$ T cells during malaria. *Immunol Rev* 293: 70-87.
8. Marshall, H. D., A. Chandele, Y. W. Jung, H. Meng, A. C. Poholek, I. A. Parish, R. Rutishauser, W. Cui, S. H. Kleinstein, J. Craft, and S. M. Kaech. 2011. Differential expression of Ly6C and T-bet distinguish effector and memory Th1 $CD4^+$cell properties during viral infection. *Immunity* 35: 633-646.
9. Fontana, M. F., de Melo, G. L., Anidi, C., Hamburger, R., Kim, C. Y., Lee, S. Y., Pham, J., and Kim, C. C. 2016. Macrophage Colony Stimulating Factor Derived from $CD4^+$ T Cells Contributes to Control of a Blood-Borne Infection. *PLoS Pathog* 12:e1006046.
10. Crotty, S. 2019. T Follicular Helper Cell Biology: A Decade of Discovery and Diseases. *Immunity* 50: 1132-1148.

11. Stephens, R., Albano, F. R., Quin, S., Pascal, B. J., Harrison, V., Stockinger, B., Kioussis, D., Weltzien, H. U., and Langhorne, J. 2005. Malaria-specific transgenic $CD4^+$ T cells protect immunodeficient mice from lethal infection and demonstrate requirement for a protective threshold of antibody production for parasite clearance. *Blood* 106:1676.
12. Stephens, R. and Langhorne, J. 2010. Effector memory Th1 CD4 T cells are maintained in a mouse model of chronic malaria. *PLoS Pathog* 6:e1001208.
13. Lundie, R. J., de Koning-Ward, T. F., Davey, G. M., Nie, C. Q., Hansen, D. S., Lau, L. S., Mintern, J. D., Belz, G. T., Schofield, L., Carbone, F. R., Villadangos, J. A., Crabb, B. S., and Heath, W. R. 2008. Blood-stage *Plasmodium* infection induces $CD8^+$ T lymphocytes to parasite-expressed antigens, largely regulated by $CD8\alpha^+$ dendritic cells. *Proc Natl Acad Sci U S A* 105:14509.
14. Kimura, D., Miyakoda, M., Honma, K., Shibata, Y., Yuda, M., Chinzei, Y., and Yui, K. 2010. Production of IFN-γ by $CD4^+$ T cells in response to malaria antigens is IL-2 dependent. *Int Immunol* 22:941.
15. Lin, J. W., Shaw, T. N., Annoura, T., Fougere, A., Bouchier, P., Chevalley-Maurel, S., Kroeze, H., Franke-Fayard, B., Janse, C. J., Couper, K. N., and Khan, S. M. 2014. The subcellular location of ovalbumin in *Plasmodium berghei* blood stages influences the magnitude of T-cell responses. *Infect Immun* 82:4654.
16. Fernandez-Ruiz, D., L. S. Lau, N. Ghazanfari, C. M. Jones, W. Y. Ng, G. M. Davey, D. Berthold, L. Holz, Y. Kato, M. H. Enders, G. Bayarsaikhan, S. H. Hendriks, L. I. M. Lansink, J. A. Engel, M. S. F. Soon, K. R. James, A. Cozijnsen, V. Mollard, A. D. Uboldi, C. J. Tonkin, T. F. de Koning-Ward, P. R. Gilson, T. Kaisho, A. Haque, B. S. Crabb, F. R. Carbone, G. I. McFadden, and W. R. Heath. 2017. Development of a Novel $CD4^+$ TCR Transgenic Line That Reveals a Dominant Role for $CD8^+$ Dendritic Cells and CD40 Signaling in the Generation of Helper and CTL Responses to Blood-Stage

Malaria. *J Immunol* 199: 4165-4179.

17. Lonnberg, T., V. Svensson, K. R. James, D. Fernandez-Ruiz, I. Sebina, R. Montandon, M. S. Soon, L. G. Fogg, A. S. Nair, U. Liligeto, M. J. Stubbington, L. H. Ly, F. O. Bagger, M. Zwiessele, N. D. Lawrence, F. Souza-Fonseca-Guimaraes, P. T. Bunn, C. R. Engwerda, W. R. Heath, O. Billker, O. Stegle, A. Haque, and S. A. Teichmann. 2017. Single-cell RNA-seq and computational analysis using temporal mixture modelling resolves Th1/Tfh fate bifurcation in malaria. *Sci Immunol* 2
18. Butler, N. S., J. Moebius, L. L. Pewe, B. Traore, O. K. Doumbo, L. T. Tygrett, T. J. Waldschmidt, P. D. Crompton, and J. T. Harty. 2011. Therapeutic blockade of PD-L1 and LAG-3 rapidly clears established blood-stage *Plasmodium* infection. *Nat Immunol* 13: 188-195.
19. McDermott, D. S., and S. M. Varga. 2011. Quantifying antigen-specific CD4 T cells during a viral infection: CD4 T cell responses are larger than we think. *J Immunol* 187: 5568-5576.
20. Akbari, M., K. Honma, D. Kimura, M. Miyakoda, K. Kimura, T. Matsuyama, and K. Yui. 2014. IRF4 in dendritic cells inhibits IL-12 production and controls Th1 immune responses against Leishmania major. *J Immunol* 192: 2271-2279.
21. Kimura, D., M. Miyakoda, K. Kimura, K. Honma, H. Hara, H. Yoshida, and K. Yui. 2016. Interleukin-27-Producing $CD4^+$ T Cells Regulate Protective Immunity during Malaria Parasite Infection. *Immunity* 44: 672-682.
22. Christiaansen, A. F., U. G. Dixit, R. N. Coler, A. Marie Beckmann, S. G. Reed, P. L. Winokur, M. B. Zimmerman, S. M. Varga, and M. E. Wilson. 2017. CD11a and CD49d enhance the detection of antigen-specific T cells following human vaccination. *Vaccine* 35: 4255-4261.
23. Malleret, B., C. Claser, A. S. Ong, R. Suwanarusk, K. Sriprawat, S. W. Howland, B.

Russell, F. Nosten, and L. Renia. 2011. A rapid and robust tri-color flow cytometry assay for monitoring malaria parasite development. *Sci Rep* 1: 118.

24. Miyakoda, M., D. Kimura, M. Yuda, Y. Chinzei, Y. Shibata, K. Honma, and K. Yui. 2008. Malaria-specific and nonspecific activation of $CD8^+$ T cells during blood stage of Plasmodium berghei infection. *J Immunol* 181: 1420-1428.
25. Bayarsaikhan, G., M. Miyakoda, K. Yamamoto, D. Kimura, M. Akbari, M. Yuda, and K. Yui. 2017. Activation and exhaustion of antigen-specific $CD8^+$ T cells occur in different splenic compartments during infection with *Plasmodium berghei*. *Parasitol Int* 66: 227-235.
26. Subramanian, A., P. Tamayo, V. K. Mootha, S. Mukherjee, B. L. Ebert, M. A. Gillette, A. Paulovich, S. L. Pomeroy, T. R. Golub, E. S. Lander, and J. P. Mesirov. 2005. Gene set enrichment analysis: a knowledge-based approach for interpreting genome-wide expression profiles. *Proc Natl Acad Sci U S A* 102: 15545-15550.
27. Wickham, H., A. Spathis, C. Chin, R. Ryan, and S. Booth. 2016. Practical management of chronic breathlessness. *BMJ* 354: h6200.
28. Kolde, R. 2019. pheatmap: Pretty Heatmaps.
29. Suzuki, S., K. Honma, T. Matsuyama, K. Suzuki, K. Toriyama, I. Akitoyo, K. Yamamoto, T. Suematsu, M. Nakamura, K. Yui, and A. Kumatori. 2004. Critical roles of interferon regulatory factor 4 in $CD11b^{high}CD8\alpha$- dendritic cell development. *Proc Natl Acad Sci U S A* 101: 8981-8986.
30. Hight-Warburton, W., and M. Parsons. 2019. Regulation of cell migration by α4 and α9 integrins. *Biochem J* 476: 705-718.
31. Anderson, K. G., K. Mayer-Barber, H. Sung, L. Beura, B. R. James, J. J. Taylor, L. Qunaj, T. S. Griffith, V. Vezys, D. L. Barber, and D. Masopust. 2014. Intravascular staining for discrimination of vascular and tissue leukocytes. *Nat Protoc* 9: 209-222.

32. Yu, Q., A. Sharma, S. Y. Oh, H. G. Moon, M. Z. Hossain, T. M. Salay, K. E. Leeds, H. Du, B. Wu, M. L. Waterman, Z. Zhu, and J. M. Sen. 2009. T cell factor 1 initiates the T helper type 2 fate by inducing the transcription factor GATA-3 and repressing interferon-gamma. *Nat Immunol* 10: 992-999.

33. Choi, Y. S., J. A. Gullicksrud, S. Xing, Z. Zeng, Q. Shan, F. Li, P. E. Love, W. Peng, H. H. Xue, and S. Crotty. 2015. LEF-1 and TCF-1 orchestrate Tfh differentiation by regulating differentiation circuits upstream of the transcriptional repressor Bcl6. *Nat Immunol* 16: 980-990.

34. Xu, L., Y. Cao, Z. Xie, Q. Huang, Q. Bai, X. Yang, R. He, Y. Hao, H. Wang, T. Zhao, Z. Fan, A. Qin, J. Ye, X. Zhou, L. Ye, and Y. Wu. 2015. The transcription factor TCF-1 initiates the differentiation of Tfh cells during acute viral infection. *Nat Immunol* 16: 991-999.

35. Ogbe, A., T. Miao, A. L. Symonds, B. Omodho, R. Singh, P. Bhullar, S. Li, and P. Wang. 2015. Early Growth Response Genes 2 and 3 Regulate the Expression of Bcl6 and Differentiation of T Follicular Helper Cells. *J Biol Chem* 290: 20455-20465.

36. Khan, O., Giles, J. R., McDonald, S., Manne, S., Ngiow, S. F., Patel, K. P., Werner, M. T., Huang, A. C., Alexander, K. A., Wu, J. E., Attanasio, J., Yan, P., George, S. M., Bengsch, B., Staupe, R. P., Donahue, G., Xu, W., Amaravadi, R. K., Xu, X., Karakousis, G. C., Mitchell, T. C., Schuchter, L. M., Kaye, J., Berger, S. L., and Wherry, E. J. 2019. TOX transcriptionally and epigenetically programs $CD8^+$ T cell exhaustion. *Nature* 571:211.

37. Alfei, F., Kanev, K., Hofmann, M., Wu, M., Ghoneim, H. E., Roelli, P., Utzschneider, D. T., von Hoesslin, M., Cullen, J. G., Fan, Y., Eisenberg, V., Wohlleber, D., Steiger, K., Merkler, D., Delorenzi, M., Knolle, P. A., Cohen, C. J., Thimme, R., Youngblood, B., and Zehn, D. 2019. TOX reinforces the phenotype and longevity of exhausted T cells in

chronic viral infection. *Nature* 571:265.

38. Johnston, R. J., A. C. Poholek, D. DiToro, I. Yusuf, D. Eto, B. Barnett, A. L. Dent, J. Craft, and S. Crotty. 2009. Bcl6 and Blimp-1 are reciprocal and antagonistic regulators of T follicular helper cell differentiation. *Science* 325: 1006-1010.
39. Nurieva, R. I., Y. Chung, G. J. Martinez, X. O. Yang, S. Tanaka, T. D. Matskevitch, Y. H. Wang, and C. Dong. 2009. Bcl6 mediates the development of T follicular helper cells. *Science* 325: 1001-1005.
40. Singh, R., T. Miao, A. L. J. Symonds, B. Omodho, S. Li, and P. Wang. 2017. Egr2 and 3 Inhibit T-bet-Mediated IFN-γ Production in T Cells. *J Immunol* 198: 4394-4402.
41. Engelhardt, B., and L. Kappos. 2008. Natalizumab: targeting α4-integrins in multiple sclerosis. *Neurodegener Dis* 5: 16-22.
42. Coisne, C., W. Mao, and B. Engelhardt. 2009. Cutting edge: Natalizumab blocks adhesion but not initial contact of human T cells to the blood-brain barrier in vivo in an animal model of multiple sclerosis. *J Immunol* 182: 5909-5913.
43. Bauer, M., Brakebusch, C., Coisne, C., Sixt, M., Wekerle, H., Engelhardt, B., and Fassler, R. 2009. Beta1 integrins differentially control extravasation of inflammatory cell subsets into the CNS during autoimmunity. *Proc Natl Acad Sci U S A* 106:1920.
44. Zander, R. A., R. Vijay, A. D. Pack, J. J. Guthmiller, A. C. Graham, S. E. Lindner, A. M. Vaughan, S. H. I. Kappe, and N. S. Butler. 2017. Th1-like Plasmodium-Specific Memory $CD4^+$ T Cells Support Humoral Immunity. *Cell Rep* 21: 1839-1852.
45. Kunzli, M., Schreiner, D., Pereboom, T. C., Swarnalekha, N., Litzler, L. C., Lotscher, J., Ertuna, Y. I., Roux, J., Geier, F., Jakob, R. P., Maier, T., Hess, C., Taylor, J. J., and King, C. G. 2020. Long-lived T follicular helper cells retain plasticity and help sustain humoral immunity. *Sci Immunol* 5: eaay5552.
46. Zander, R. A., Obeng-Adjei, N., Guthmiller, J. J., Kulu, D. I., Li, J., Ongoiba, A., Traore,

B., Crompton, P. D., and Butler, N. S. 2015. PD-1 Co-inhibitory and OX40 Co-stimulatory Crosstalk Regulates Helper T Cell Differentiation and Anti-*Plasmodium* Humoral Immunity. *Cell Host Microbe* 17:628.

47. Obeng-Adjei, N., S. Portugal, T. M. Tran, T. B. Yazew, J. Skinner, S. Li, A. Jain, P. L. Felgner, O. K. Doumbo, K. Kayentao, A. Ongoiba, B. Traore, and P. D. Crompton. 2015. Circulating Th1-Cell-type Tfh Cells that Exhibit Impaired B Cell Help Are Preferentially Activated during Acute Malaria in Children. *Cell Rep* 13: 425-439.

Figure Legends

Figure 1. Both CD11a^{hi}CD49d^{hi} and CD11a^{hi}CD49d^{lo} *Plasmodium*-specific CD4^{+} T cells increase after infection with *P. chabaudi*

C57BL/6 mice received a transfer of PbT-II cells, were infected with *P. chabaudi* or not infected (Uninf), and PbT-II cells from spleens and peripheral blood lymphocytes (PBLs) were stained 7, 9, 14, and 30 d after infection.

(A) Levels of parasitemia in mice used for the analysis.

(B) Splenocytes (upper) and PBLs (lower) were stained for CD4, CD3, CD45.1, CD45.2, CD11a, and CD49d. CD45.2/CD45.1 profiles of CD3^{+}CD4^{+} cells and CD11a/CD49d profiles of PbT-II (CD45.1^{+}CD3^{+}CD4^{+}) cells are shown. Numbers indicate the proportion (%) of each population within the square.

(C) Summary of PbT-II subpopulations from the spleen (upper and middle panel) and PBLs (lower panel) of mice uninfected (day 7 after transfer) or infected with *P. chabaudi* for 7, 9, 14, and 30 d. The proportions and number of PbT-II cells in spleen (left panel) and those of CD11a^{hi}CD49d^{hi} (red), CD11a^{hi}CD49d^{lo} (blue), and CD11a^{lo}CD49d^{lo} (black) among PbT-II cells are plotted (right panel). Comparison of the values in infected mice to those in uninfected mice was analyzed using two-way ANOVA followed by Tukey's multiple comparison post hoc test. *, $p< 0.05$; ***, $p<0.001$.

Representative data (3 mice/group) of two independent experiments with similar results are shown.

Figure 2. CD11a^{hi}CD49d^{hi} and CD11a^{hi}CD49d^{lo} PbT-II cells proliferate similarly

(A) C57BL/6 mice received a transfer of CFSE-labeled PbT-II cells (1×10^6), were infected with *P. chabaudi*, and then their splenocytes were analyzed 3–6 d later. Splenocytes were stained for CD4, CD3, CD45.1, CD11a, and CD49d and CD4/CD45.1 profiles of CD3$^+$CD4$^+$ cells and CD11a/CD49d profiles of PbT-II (CD45.1$^+$CD3$^+$CD4$^+$) cells are shown (upper panel). Numbers indicate proportions (%) of cells in each square. CFSE profiles of CD11a^{hi}CD49d^{hi}, CD11a^{hi}CD49d^{lo}, and CD11a^{lo}CD49d^{lo} PbT-II cells are shown (lower panel). Numbers indicate proportions of CFSE^{lo} cells.

(B) Summary of parasitemia levels, proportions of PbT-II cells in splenic CD4$^+$ T cells, and the proportions of CFSE^{lo} cells in CD11a^{hi}CD49d^{hi} (red), CD11a^{hi}CD49d^{lo} (blue), and CD11a^{lo}CD49d^{lo} (black) PbT-II cells are shown. Comparison of the values in CD11a^{hi}CD49d^{hi} and CD11a^{hi}CD49d^{lo} cells to those in CD11a^{lo}CD49d^{lo} cells were analyzed using two-way ANOVA followed by Tukey's multiple comparison post hoc test. *, $p< 0.05$; ***, $p<0.001$. Representative results of two independent experiments are shown (3 mice/group per experiment).

Figure 3. CD11a^{hi}CD49d^{hi} and CD11a^{hi}CD49d^{lo} PbT-II cells localize in different splenic compartments

(A) C57BL/6 mice were adoptively transferred with PbT-II cells and infected with *P. chabaudi*. Seven days later, the mice received PE-anti-CD45.1 mAb 3 min prior to euthanasia. The spleen cells were stained for CD45.2, CD4, CD3, Vα2, CD11a, and CD45 and analyzed using flow cytometry. Gating strategy and CD45.1 staining profile of CD11a^{hi}CD49d^{hi} and CD11a^{hi}CD49d^{lo}-gated PbT-II (CD4$^+$CD45.2$^-$) cells is shown (center). Proportions (%) of CD45.1$^+$ cells (blue, spleen red pulp/marginal zone) and

CD45.1^{-} cells (red, spleen white pulp) in CD49d^{hi} and CD49d^{lo} PbT-II cells are shown (right). Numbers indicate proportions (%) of cells in each square. Statistical analysis was performed using unpaired two-tailed Student's *t* test: **, $p< 0.01$.

(B) Seven days after infection, spleens were removed, sectioned, fixed, and stained with PE-anti-CD45.1, FITC-anti-CD169, and biotin-anti-CD49d plus Cy5-streptavidin. Cy5 (CD49d) was merged with PE (CD45.1) to extract CD45.1^{+}CD49d^{+} PbT-II cells (CD49d^{+}PbT-II, purple) and CD45.1^{-}CD49d^{+} cells were excluded from the analysis. CD45.1^{+}CD49d^{-}cells (CD49d^{-}PbT-II, blue) and CD169^{+} cells (green) are shown. The proportions of PbT-II cells in spleen red pulp/marginal zone (RP/MZ) and spleen white pulp (WP) are shown (right). Representative results of two independent experiments (3 mice/group per experiment). Statistical analysis was performed using unpaired two-tailed Student's *t* test: **, $p< 0.01$.

Figure 4. Transcriptional profiling of CD11a^{hi}CD49d^{hi} and CD11a^{hi}CD49d^{lo} PbT-II cells

Transcriptional profiling suggests functional bifurcation of CD11a^{hi}CD49d^{hi} and CD11a^{hi}CD49d^{lo} PbT-II cells towards Th1 and Tfh cells. C57BL/6 mice were transferred with PbT-II cells and then infected with *P. chabaudi*. Seven days after infection, CD11a^{hi}CD49d^{hi} and CD11a^{hi}CD49d^{lo} PbT-II cells were sorted and purified from infected mice and CD11a^{lo}CD49d^{lo} PbT-II cells were purified from uninfected PbT-II mice. RNA was prepared from the cells purified from individual mice and subjected to microarray analysis.

(A) Principle compartment analysis of CD11a^{hi}CD49d^{hi} PbT-II cells (red), CD11a^{hi}CD49d^{lo} PbT-II cells (blue), and CD11a^{lo}CD49d^{lo} (black) PbT-II cells prepared from individual mice. Each dot represents PbT-II cells prepared from an individual mouse.

(B) Volcano plots of differentially expressed genes between CD11a^{hi}CD49d^{hi} PbT-II cells and

CD11a^{hi}CD49d^{lo} PbT-II cells (p<0.05). Genes upregulated in CD11a^{hi}CD49d^{hi} PbT-II cells (red) and upregulated in CD11a^{hi}CD49d^{lo} PbT-II cells (blue) are shown.

(C) Heatmap of genes upregulated and downregulated in CD11a^{hi}CD49^{hi} PbT-II cells when compared with CD11a^{hi}CD49^{lo} PbT-II cells. Representative genes of Th1 and Tfh cell lineages are selected.

(D) Gene set enrichment analysis (GSEA) of gene signatures upregulated (upper panel) and downregulated (lower panel) in CD11a^{hi}CD49d^{hi} PbT-II cells relative to their expression in CD11a^{hi}CD49d^{lo} PbT-II cells from the published database Molecule Signature Database (dataset: GSE43863).

Figure 5. Fluorescence activated cell sorting analysis of CD49d^{hi} and CD49d^{lo} PbT-II cells

CD49d^{hi} and CD49d^{lo} PbT-II cells exhibit Th1-like and Tfh-like phenotypes. C57BL/6 mice received a transfer of PbT-II cells, were infected with *P. chabaudi,* and their splenocytes were analyzed 7 d later. Spleen cells were stained for CD3, CD4, CD11a, CD49d, and CD45.1, as well as other cell surface or intracellular markers.

(A) Gating strategy.

(B) Profiles of marker/CD49d in host (CD45.1^{-}) CD11a^{lo} CD4^{+} T cells, host CD11a^{hi} CD4^{+} T cells, and PbT-II (CD45.1^{+}CD3^{+}CD4^{+}) cells are shown.

Representative result of 3 independent experiments with similar results (3 mice/group per experiment).

Figure 6. CD49d^{hi} and CD49d^{lo} PbT-II cells produce different cytokines

Mice received a transfer of PbT-II cells and were subsequently infected with *P. chabaudi*.

(A) Seven days later, CD49d^{hi} and CD49d^{lo}PbT-II cells (5×10^3) were sorted and purified from pooled spleen cells of four mice and cultured in the presence of uninfected C57BL/6 spleen cells (5×10^5) or PbT-II peptides for 2 d. Cytokine levels in the culture supernatant were determined using ELISA. Representative results of two independent experiments with similar results are shown.

(B) Seven days later, spleen cells were cultured in the presence of PMA and ionomycin (left) or PbT-II peptide (right) for 4 h. Cells were stained for CD3, CD4, CD11a, CD49d, and CD45.1, fixed and permeabilized, and intracellularly stained for the indicated cytokines. IFN-γ, TNF-α, IL-10 and IL-2 were stained in the same tube. Summary of the statistical analysis is shown to the right.

Statistical analysis was performed using paired two-tailed Student's *t* test. *, $p< 0.05$, **, $p< 0.01$, *** $p< 0.001$.

Figure 7. CD49d^{lo} PbT-II cells can develop into functional Th1 cells

C57BL/6 mice received a transfer of PbT-II cells and were subsequently infected with *P. chabaudi*. Seven days later, spleen cells were stained for CD3, CD4, CD11a, and CD49d and CD11a^{hi}CD49d^{hi} and CD11a^{hi}CD49d^{lo} PbT-II cells (CD3$^+$CD4$^+$CD45.1$^+$) were purified via sorting. The sorted cells (2×10^5) were transferred into naïve C57BL/6 mice, which were then

intravenously administered with BM-DCs pulsed with PbT-II peptide on the next day. Spleen cells were analyzed 2, 4, and 5 days after stimulation using a flow cytometer.

(A) Experimental procedure schematic and profiles of sorted $CD11a^{hi}CD49d^{hi}$ and $CD11a^{hi}CD49d^{lo}$ PbT-II cells, which were transferred into recipient C57BL/6 mice.

(B, C) Spleen cells from mice receiving a transfer of $CD49d^{hi}$ and $CD49d^{lo}$ PbT-II cells were stained for CD3, CD4, CD45.1, CD11a, CD49d, PD-1/LAG3, Cy6C/CXCR5, or intracellularly for IL-2/IFN-γ at 2 and 4 days (B) or 5 days (C) after *in vivo* stimulation and analyzed using a flow cytometer. For intracellular cytokine staining, spleen cells were cultured in the presence of PMA and ionomycin for 4 h, stained for CD3, CD4, CD45.1, CD11a, and CD49d, fixed and permeabilized, and stained for IL-2 and IFN-γ (C). The numbers in the profiles indicate the proportions of cells in the square or in each quadrant.

(D, E) Summary of the proportions and numbers of PbT-II cells, and the proportions of $CD49d^{hi}$ cells within the PbT-II cells 2 days (D) and 5 days (E) after *in vivo* stimulation are shown. Numbers of PbT-II cells were calculated by multiplying the proportion of PbT-II cells by the number of total spleen cells. Statistical analysis was performed using unpaired two-tailed Student's *t* test: NS, Not significant; *, $p< 0.05$.

Data are presented as a summary of three independent experiments with similar results (3 mice/group).

Figure 8. Maintenance of CD49d^{hi} and CD49d^{lo} PbT-II cells during *P. chabaudi* infection

C57BL/6 mice received a transfer of PbT-II cells and were subsequently infected with *P. chabaudi*. Seven days later, CD49d^{hi} and CD49d^{lo} PbT-II cells were sorted and purified from spleens and transferred into C57BL/6 mice (2× 10^5/mouse), which had been infected with *P. chabaudi* for 5 d. After 2 d, spleen cells were analyzed using flow cytometry.

(A) Experimental procedure schematic and profiles of sorted CD11a^{hi}CD49d^{hi} and CD11a^{hi}CD49d^{lo} PbT-II cells, which were transferred into recipient C57BL/6 mice.

(B) Spleen cells from the mice transferred with CD49d^{hi} PbT-II cells (upper panel) and CD49d^{lo} PbT-II cells (lower panel) were stained for CD4, CD45.1, CD11a, CD49d, PD-1, CXCR5, LAG3, or Ly6C and analyzed using a flow cytometer. The numbers in the profiles indicate the proportions of cells in the square or in each quadrant.

(C) Summary of the proportions of cells expressing each marker in CD49d^{hi} PbT-II cells (red) and CD49d^{lo} PbT-II cells (blue). Statistical analysis was performed using unpaired two-tailed Student's *t* test: NS, not significant, **, p<0.01, ***, p< 0.001. Data are representative of two independent experiments with similar results (3 mice/group).

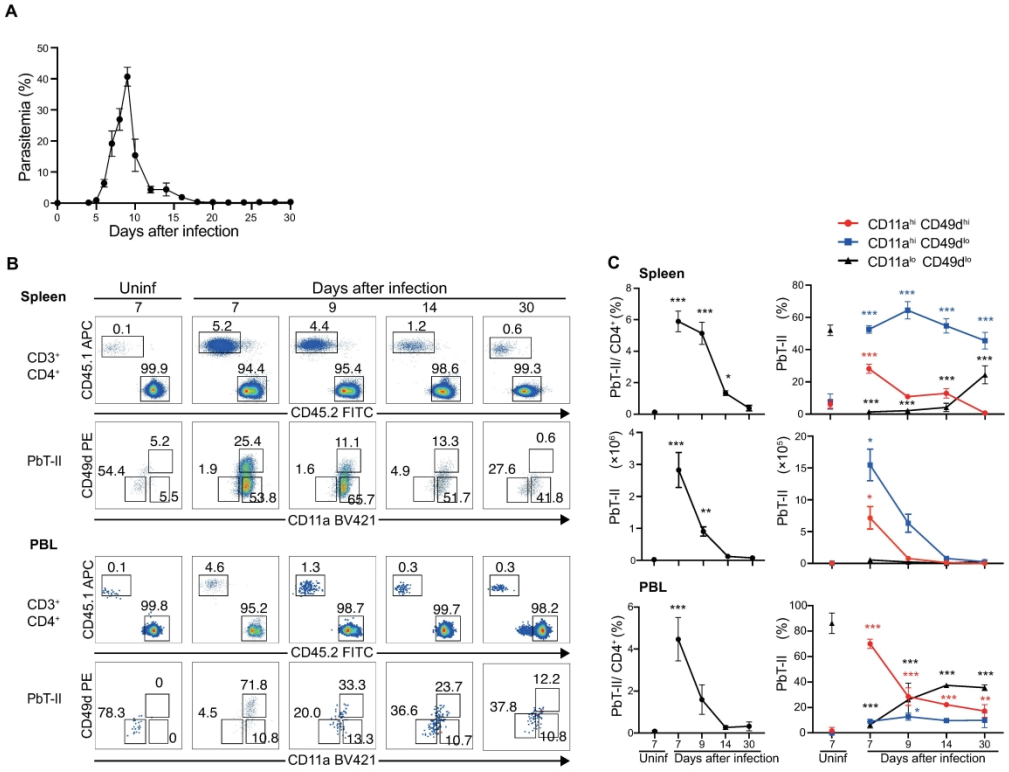

Figure 1

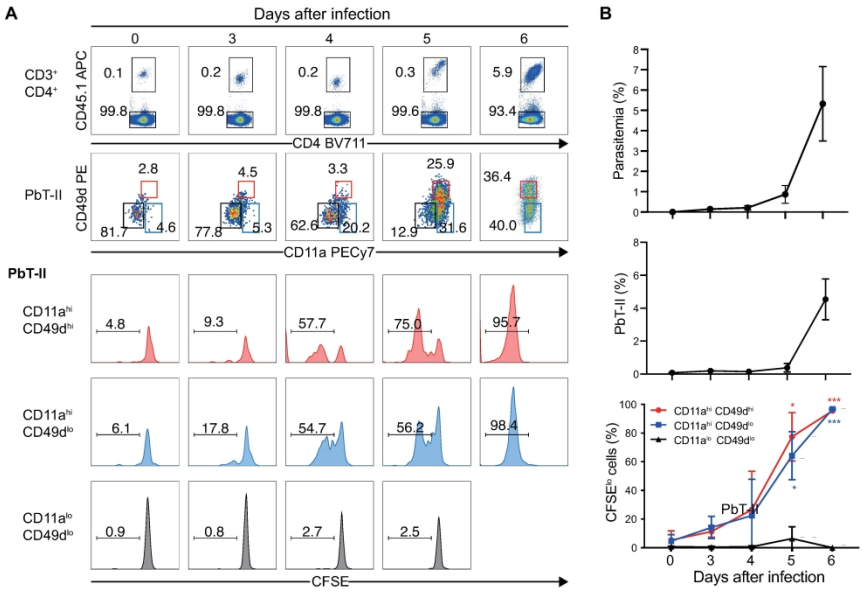

Figure 2

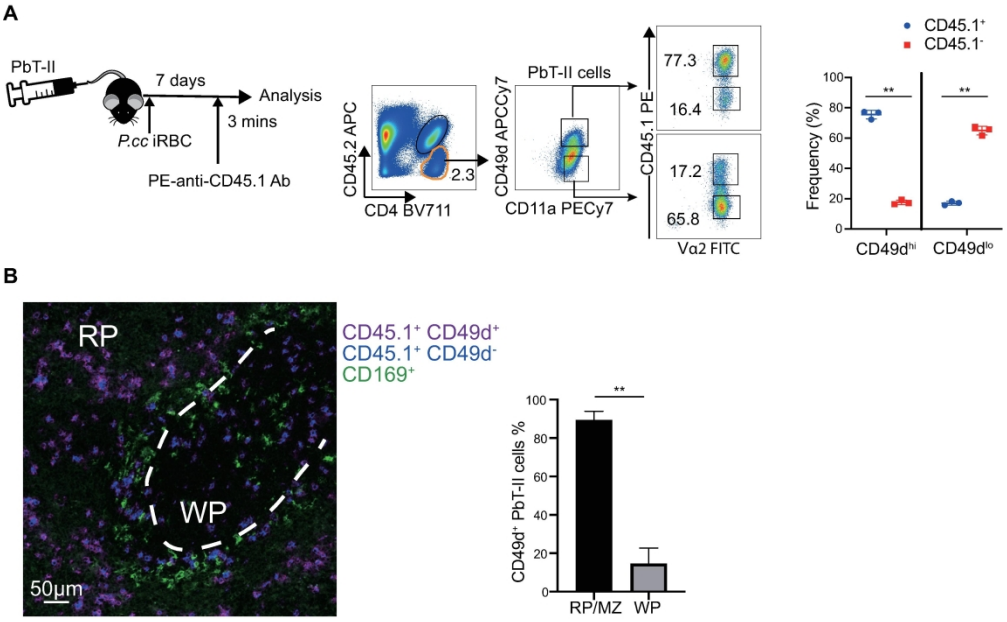

Figure 3

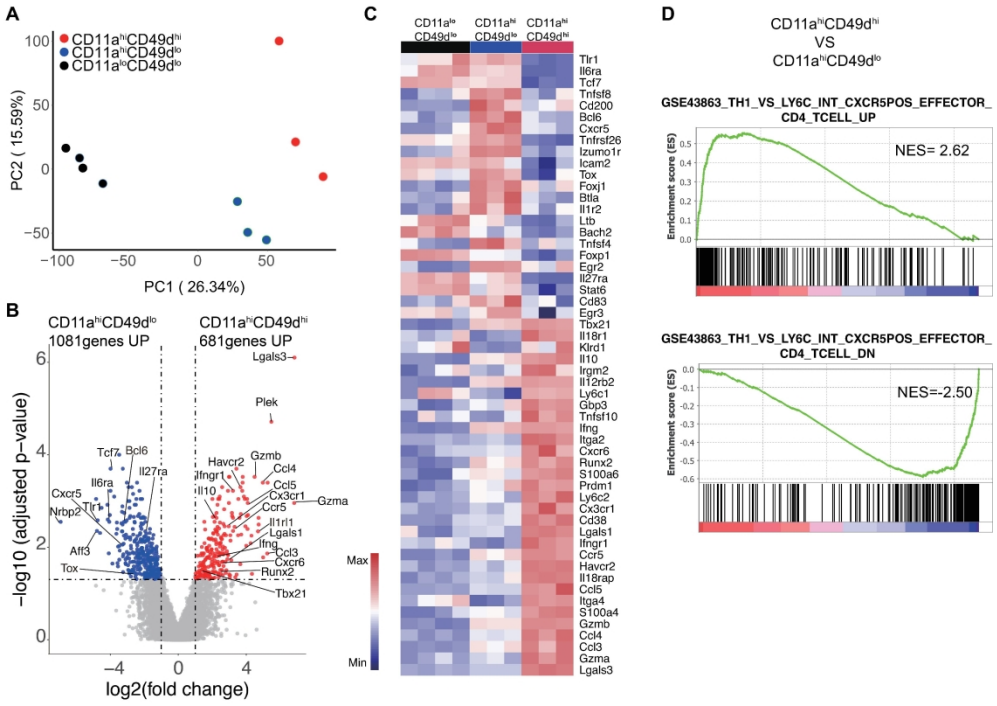

Figure 4

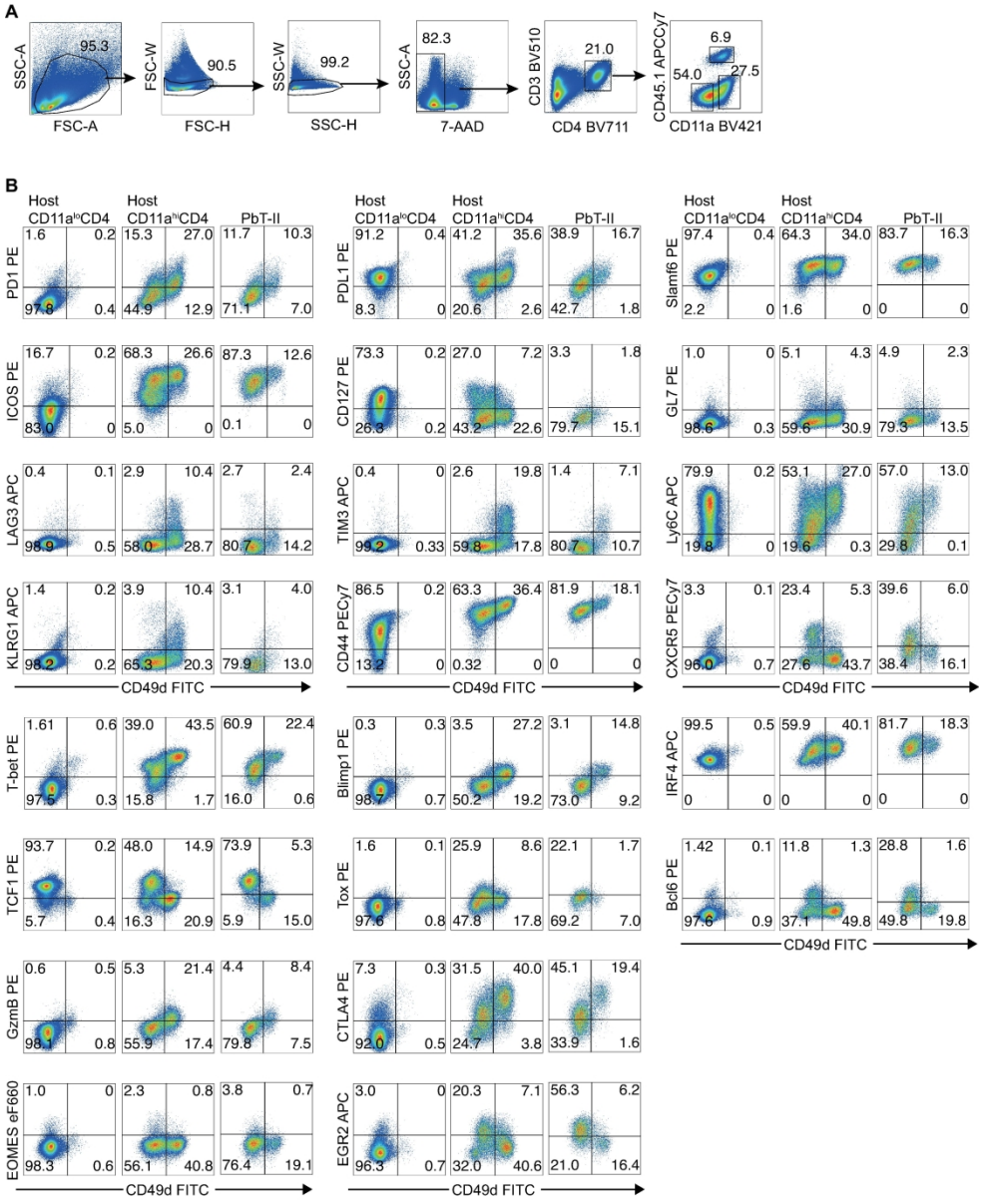

Figure 5

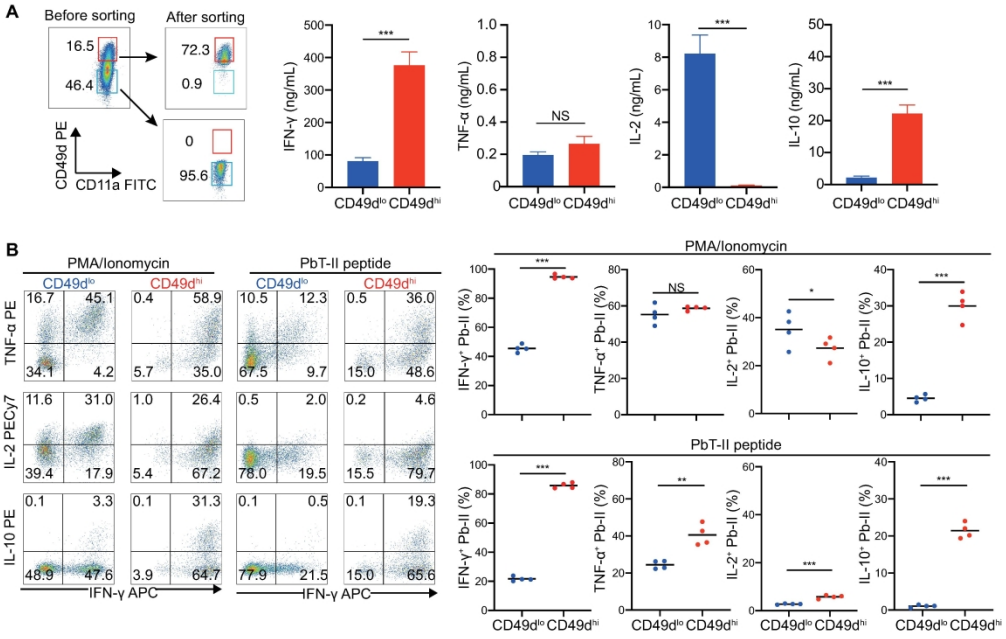

Figure 6

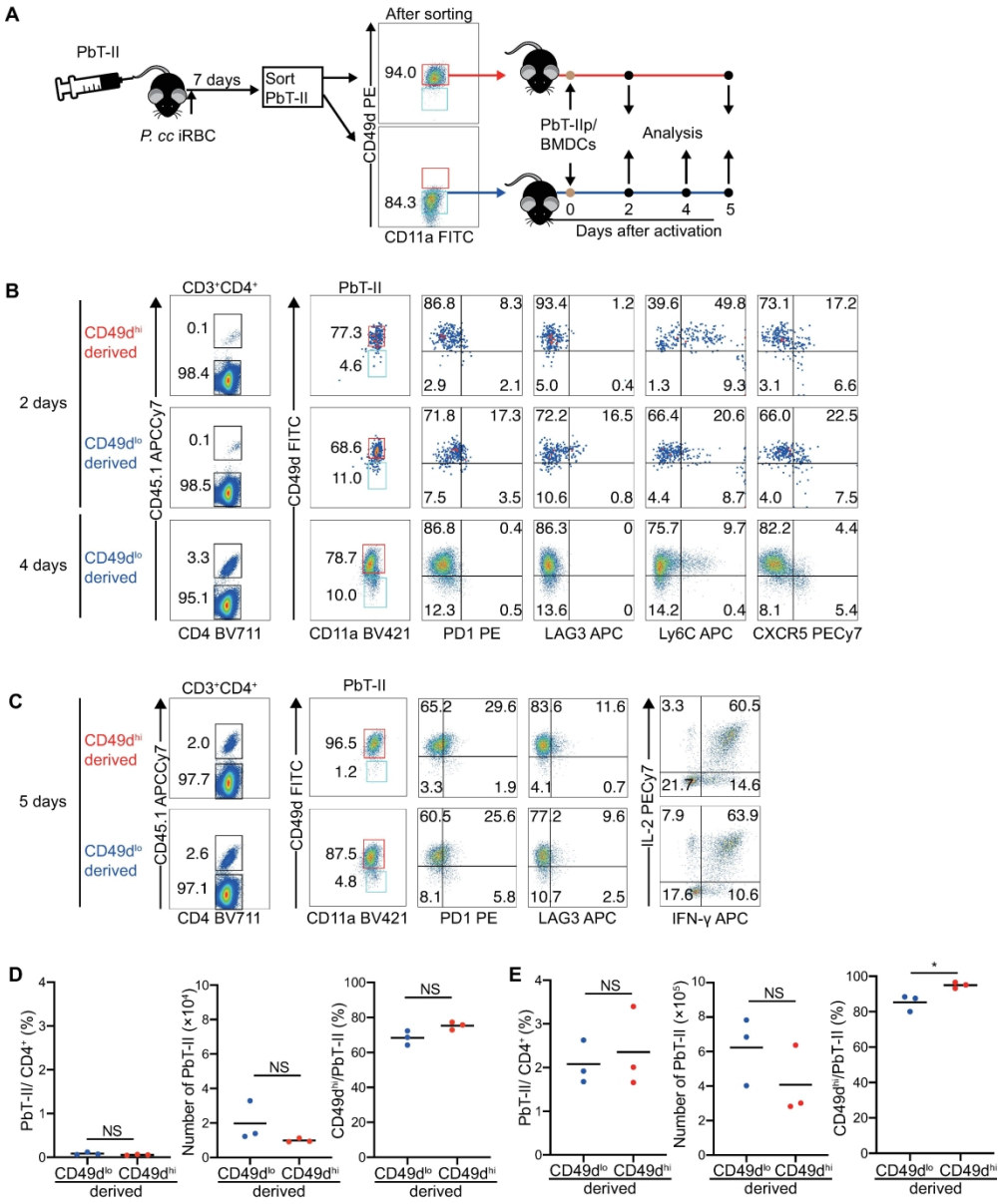

Figure 7

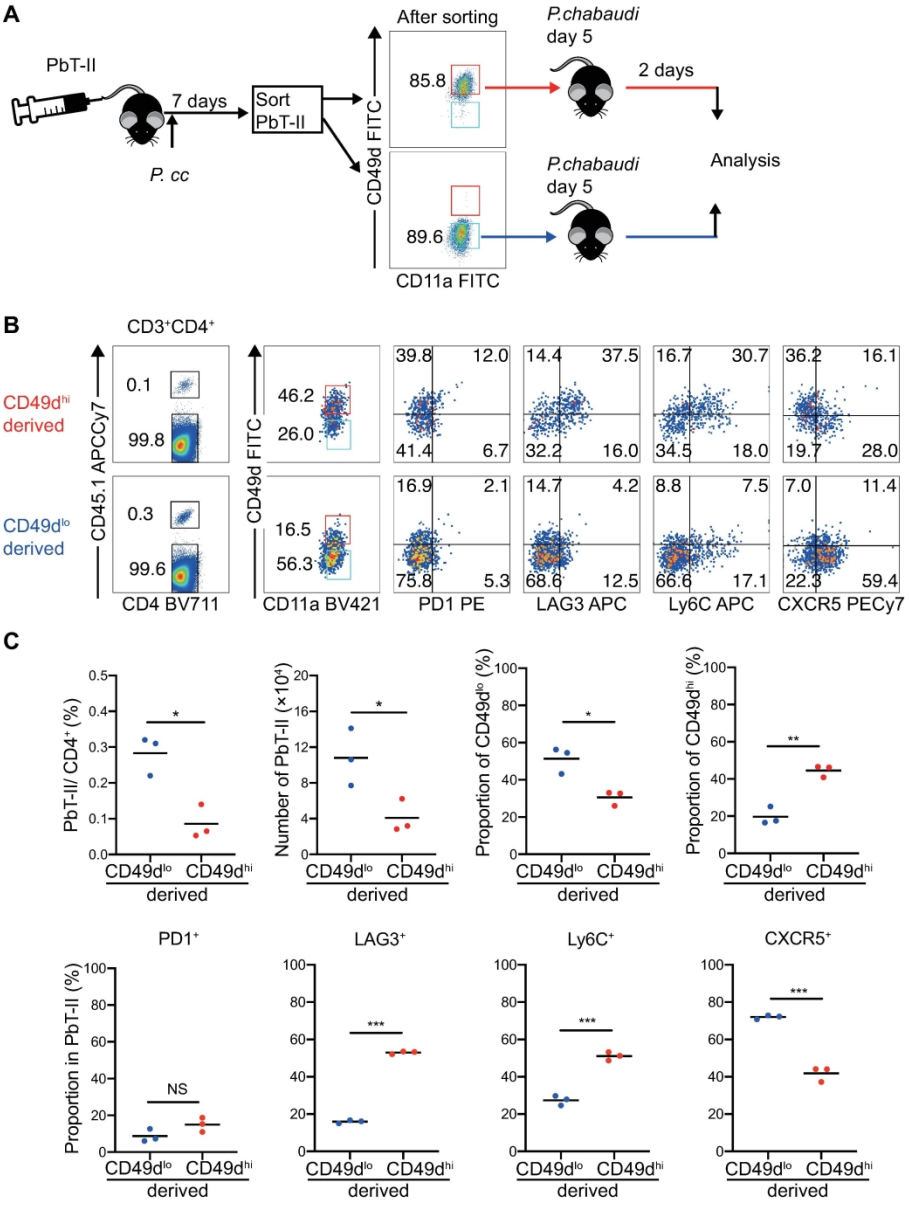

Figure 8